

d-Wave Surface Altermagnetism in Centrosymmetric Collinear Antiferromagnets

Ersoy Şaşioğlu^{1,*}, Ingrid Mertig¹, and Samir Lounis¹

¹*Institute of Physics and Halle-Berlin-Regensburg Cluster of Excellence CCE,
Martin Luther University Halle-Wittenberg, 06120 Halle (Saale), Germany*

(Dated: February 10, 2026)

Broken inversion symmetry at the surfaces of centrosymmetric collinear antiferromagnets lifts the combined inversion and time-reversal symmetry (PT) and can generate nonrelativistic d -wave spin splitting, termed surface altermagnetism. Combining symmetry analysis with first-principles calculations, we show that surface inversion breaking, while necessary, is not sufficient for this effect. Surface altermagnetism emerges only when the surface termination simultaneously breaks both PT and translation-time-reversal symmetry (tT), thereby inducing magnetic sublattice inequivalence between antiferromagnetically coupled surface moments. We demonstrate this mechanism explicitly for the G -type antiferromagnets V_3Al and $BaMn_2Sb_2$, and show that the same symmetry criterion applies broadly across distinct structural families of centrosymmetric antiferromagnets. These results establish a general, symmetry-based route to realizing robust, exchange-driven spin polarization at antiferromagnetic surfaces and interfaces.

Antiferromagnets (AFMs) possessing combined inversion and time-reversal symmetry (PT) exhibit spin-degenerate electronic bands in the absence of spin-orbit coupling (SOC). The recent discovery of altermagnetism has challenged this paradigm by demonstrating that collinear compensated magnets can host large nonrelativistic spin splittings when their magnetic space groups break PT while preserving the equivalence of opposite-spin sublattices through crystal rotations or mirror operations [1–3]. The resulting momentum-dependent spin polarization follows characteristic d -, g -, or i -wave symmetries dictated by the underlying lattice and has been realized in several classes of transition-metal compounds [4–9]. Experimentally, altermagnetic band splittings have now been directly resolved in α -MnTe, CrSb, and the metallic room-temperature d -wave altermagnet KV_2Se_2O using angle-resolved photoemission spectroscopy and complementary transport probes, establishing altermagnets as a distinct class of compensated magnets with nonrelativistic spin polarization [10–13]. Motivated by this discovery, altermagnetism has rapidly evolved into an active research field, encompassing symmetry-based classifications, large-scale materials screening, and first-principles studies of bulk and low-dimensional systems [14–28].

An important and largely unexplored question is whether analogous altermagnetic spin splitting can also emerge at the *surfaces* of otherwise PT -symmetric AFMs. While recent theoretical and materials-driven studies have firmly established altermagnetism in bulk and low-dimensional periodic systems, the role of surfaces, where translational symmetry is explicitly broken, remains poorly understood. Recent theoretical work has begun to examine surface electronic structures of intrinsically altermagnetic bulk materials [29]; however, the emergence of altermagnetic spin splitting at the surfaces of bulk PT -symmetric AFMs, where altermagnetism is absent in the bulk, has not been established. Surface ter-

mination inherently breaks inversion symmetry and thus lifts PT even in centrosymmetric C - and G -type AFMs whose bulk bands are strictly spin-degenerate. Unlike relativistic Rashba or Dresselhaus effects, which originate from SOC in noncentrosymmetric crystals [30, 31], any surface-induced spin splitting in AFMs would be purely exchange-driven and rooted in the local magnetic environment. Whether surface-induced inversion breaking alone is sufficient to generate a symmetry-dictated, momentum-dependent spin polarization analogous to that of bulk altermagnets, or whether additional symmetry constraints remain operative at the surface, therefore remains an open question.

In this Letter, we show that crystallographic symmetry breaking at antiferromagnetic surfaces, although necessary, is not sufficient to induce surface altermagnetism. Instead, a further degeneracy-protecting symmetry must be removed: the surface termination must break translation-time-reversal symmetry (tT), thereby inducing magnetic sublattice inequivalence between antiferromagnetically coupled surface moments. Using first-principles calculations combined with symmetry analysis, we demonstrate this mechanism for representative centrosymmetric collinear AFMs with G -type magnetic order, including cubic $L2_1$ -type Heuslers (V_3Al) and tetragonal 122 pnictides ($BaMn_2Sb_2$), and show that the same symmetry criterion applies broadly across distinct structural families of centrosymmetric AFMs. In all cases, the bulk ground state preserves PT symmetry and exhibits strictly spin-degenerate electronic bands.

For surface terminations that break the equivalence of the two antiferromagnetic sublattices, symmetry analysis constrains the leading nonrelativistic spin splitting of the surface states to transform according to a d -wave representation, corresponding to the lowest-order irreducible representation allowed by the surface magnetic point group [2, 5]. Using first-principles calculations, we demonstrate that this symmetry-allowed spin split-

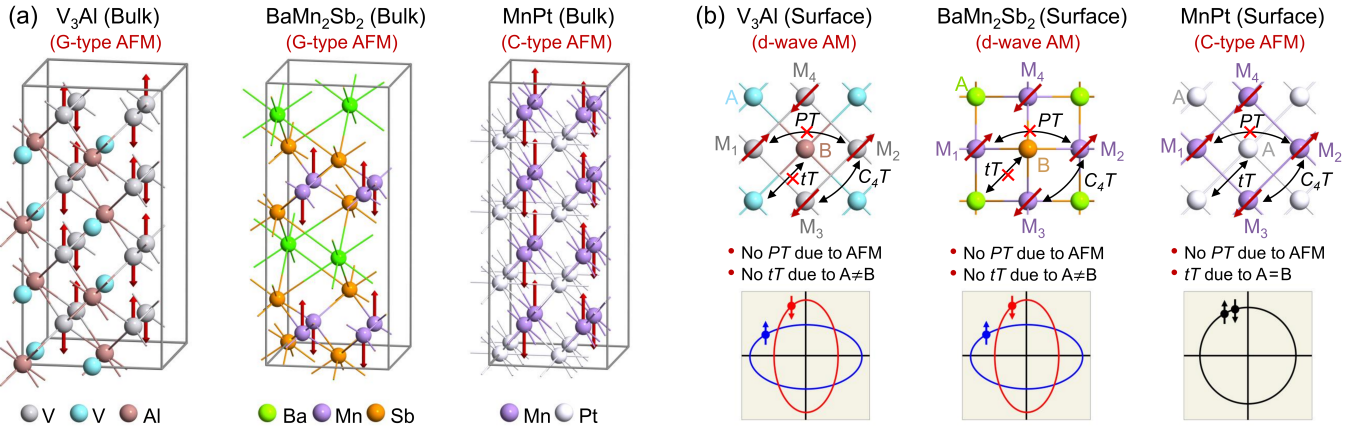


FIG. 1. Bulk and surface magnetic structures and symmetry conditions. (a) Bulk magnetic configurations of the centrosymmetric AFMs V_3Al and $BaMn_2Sb_2$ (G -type) and $MnPt$ (C -type). All bulk phases preserve combined PT symmetry, enforcing spin-degenerate electronic bands in the absence of spin-orbit coupling. Arrows indicate magnetic moment orientations. (b) Top view of the surface and subsurface layers at a representative surface termination. The surface is taken along the (001) direction of the bulk unit cell, for which each atomic layer contains two antiferromagnetically coupled magnetic atoms. For V_3Al and $BaMn_2Sb_2$, the surface layers form a checkerboard arrangement that breaks the equivalence of the two antiferromagnetically coupled surface sublattices ($A \neq B$), thereby breaking both PT and tT symmetry. Although a fourfold rotation combined with time reversal (C_4T) remains, this symmetry does not enforce spin degeneracy, allowing a symmetry-permitted nonrelativistic d -wave altermagnetic spin splitting, schematically indicated by the surface Fermi surfaces. In contrast, the $MnPt$ surface preserves tT symmetry despite broken inversion and therefore remains spin-degenerate. The indicated symmetry operations summarize the distinct symmetry constraints in each case.

ting indeed emerges at realistic antiferromagnetic surfaces, exhibits a characteristic momentum dependence, and is strongly confined to the outermost magnetic layers. These results establish centrosymmetric AFMs as a previously unexplored platform for nonrelativistic surface and interface altermagnetism. In contrast to bulk altermagnets, where spin splitting is constrained by crystal rotations or mirror symmetries combined with time reversal, surface altermagnetism is governed by the breaking or survival of tT symmetry within the surface plane.

To elucidate the symmetry mechanism responsible for this effect, Fig. 1 summarizes the origin of surface altermagnetism by contrasting bulk and surface magnetic structures of representative centrosymmetric AFMs. All materials considered are collinear C - or G -type AFMs that preserve combined PT symmetry in the bulk. As shown in Fig. 1(a), the bulk magnetic structures of V_3Al , $BaMn_2Sb_2$, and $MnPt$ are fully compensated and antiferromagnetically ordered. In the following, we focus on the (001) surface, for which each magnetic layer contains two antiferromagnetically coupled magnetic moments.

At a surface, inversion symmetry is inherently broken and the combined PT symmetry is therefore absent even for centrosymmetric AFMs. However, as illustrated in Fig. 1(b), the absence of PT alone is not sufficient to generate altermagnetic spin polarization. Spin degeneracy can still be enforced by additional symmetries that relate opposite-spin magnetic moments within the surface plane. In particular, spin degeneracy survives if the surface magnetic structure preserves tT symmetry, where

a half translation t exchanges the two antiferromagnetic sublattices.

The role of these symmetries is made explicit in the top views of the surface and subsurface layers shown in Fig. 1(b). The magnetic atoms are labeled M_1 and M_2 (spin-up) and M_3 and M_4 (spin-down), while nonmagnetic atoms in the surface unit cell are denoted by A and B . For V_3Al and $BaMn_2Sb_2$, the surface termination breaks inversion symmetry, as indicated by the absence of a PT operation that maps the two spin-up magnetic moments M_1 and M_2 onto each other. At the same time, the checkerboard arrangement of the surface and subsurface layers renders the nonmagnetic sites A and B inequivalent, such that no half translation exists that exchanges them. As a consequence, tT symmetry is also broken. Although a fourfold rotation combined with time reversal (C_4T) remains and maps M_3 onto M_2 , this symmetry does not exchange the two spin-polarized surface sublattices and therefore does not enforce spin degeneracy. With both PT and tT absent, the surface electronic states are free to develop a nonrelativistic, momentum-dependent spin splitting characteristic of surface altermagnetism.

In contrast, for $MnPt$ the nonmagnetic surface sites A and B are equivalent (both corresponding to Pt atoms), such that a half translation exchanging them remains a symmetry of the surface. Accordingly, tT symmetry is preserved despite the absence of inversion symmetry. The survival of tT enforces spin degeneracy of the surface electronic structure, making $MnPt$ a conventional AFM

at the surface with no altermagnetic spin splitting. This example highlights that surface inversion breaking alone does not guarantee surface altermagnetism; the equivalence or inequivalence of antiferromagnetically coupled surface sublattices is decisive.

The symmetry criterion identified above has direct implications for materials selection. Table I illustrates its generality by surveying representative compounds from the major classes of centrosymmetric collinear AFMs considered in this work (an extended list is provided in the Supplemental Material [32]). Although all listed materials possess centrosymmetric bulk crystal structures and comparable surface space groups, surface altermagnetism emerges only when the surface termination simultaneously breaks PT and tT symmetry, thereby lifting the equivalence of antiferromagnetically coupled surface sublattices. In materials such as MnPt, LaFeO₃, and K₂NiF₄, a half translation remains that exchanges equivalent surface sites, preserving tT symmetry and enforcing spin degeneracy despite broken inversion symmetry. Together, Fig. 1 and Table I establish the simultaneous breaking of PT and tT as the defining symmetry condition for surface altermagnetism in collinear AFMs and provide a practical guideline for identifying candidate materials.

We now test this symmetry-based criterion at the microscopic level using first-principles electronic-structure calculations for representative AFMs that satisfy the surface symmetry conditions for altermagnetism. We focus on the G-type AFMs V₃Al and BaMn₂Sb₂, identified in Fig. 1 and Table I as prototypical systems in which surface altermagnetism is symmetry-allowed. The calculations are based on density-functional theory within the generalized gradient approximation, treating magnetism in the collinear and nonrelativistic limit [33–35]. Surface electronic structures are obtained from slab geometries constructed along the (001) surface orientation. In symmetric slabs, the two opposing surface terminations are related by the underlying G-type antiferromagnetic order, such that partner surface states on opposite sides exhibit opposite spin polarizations. As a result, their spin splittings compensate in the total spectrum, preserving global spin degeneracy. While the underlying splitting can always be recovered from surface- or layer-resolved projections, for clarity of presentation we therefore employ asymmetric slab geometries in which the altermagnetic splitting appears directly in the total band structure. Corresponding results for symmetric slabs, as well as further computational details, are provided in the Supplemental Material [32]. SOC is neglected in order to isolate the purely exchange-driven origin of the observed spin splitting.

Figure 2(a) shows the bulk and surface band structures of V₃Al along the in-plane X–Γ–Y high-symmetry path, using an orthorhombic surface Brillouin zone with $a = b$. V₃Al is a high- T_N antiferromagnet, with reported

TABLE I. Representative centrosymmetric collinear AFMs illustrating the necessary condition for surface altermagnetism (see Supplementary Material for an extended list and symmetry and crystallographic analysis). All materials preserve combined PT symmetry in the bulk and therefore exhibit spin-degenerate bulk electronic bands in the absence of SOC. Surface altermagnetism (AM) is symmetry-allowed only when tT symmetry is broken at the surface.

Material	Class	AFM type	tT broken	AM
V ₃ Al	L2 ₁ Heusler	G-type	Yes	Yes
BaMn ₂ Sb ₂	122 pnictide	G-type	Yes	Yes
MnPt	L1 ₀ intermetallic	C-type	No	No
LaMnPO	1111 oxypnictide	C-type	No	No
LaFeO ₃	Perovskite oxide	G-type	No	No
K ₂ NiF ₄	Layered perovskite	C-type	No	No

Néel temperatures of the order of 600 K, and has been discussed as a spin-gapless AFM [36–39]. In the bulk reference calculation, the electronic bands are strictly spin-degenerate and exhibit a Dirac-like dispersion near the X point, with the Dirac node located approximately 60 meV below the Fermi level. At the surface, pronounced non-relativistic spin splitting emerges in states localized near the outermost magnetic layers. The Dirac cones shift toward the X and Y points and are pinned close to the Fermi level, with each linear branch carrying opposite spin polarization. The resulting altermagnetic spin splitting reaches values of up to 0.32 eV, giving rise to metallic Dirac surface states with a strong momentum-dependent spin polarization.

An electronically distinct manifestation of surface altermagnetism is found in BaMn₂Sb₂, shown in Fig. 2(b). BaMn₂Sb₂ is a layered antiferromagnetic semiconductor with a small bulk band gap of about 0.3 eV and a reported Néel temperature of approximately 450 K [40–42]. While the bulk electronic structure remains fully spin-degenerate, the surface band structure develops two Dirac points located approximately 20 meV above the Fermi level along the Γ–X and Γ–Y directions. These Dirac states are fully spin-polarized in a momentum-selective manner: bands along Γ–X carry one spin character, whereas those along Γ–Y carry the opposite spin. The resulting altermagnetic spin splitting reaches values of up to ∼0.35 eV near the Fermi level, demonstrating that pronounced nonrelativistic spin polarization can emerge even at the surface of a small-gap antiferromagnetic semiconductor, in sharp contrast to its spin-degenerate bulk electronic structure.

The anisotropic spin polarization of the surface bands discussed above has a direct manifestation in momentum space at the Fermi level. These momentum-space signatures of surface altermagnetism are illustrated in Fig. 2(c) and Fig. 2(d), which show spin-resolved two-dimensional surface Fermi surfaces obtained from asymmetric slab calculations. In BaMn₂Sb₂, only two surface-

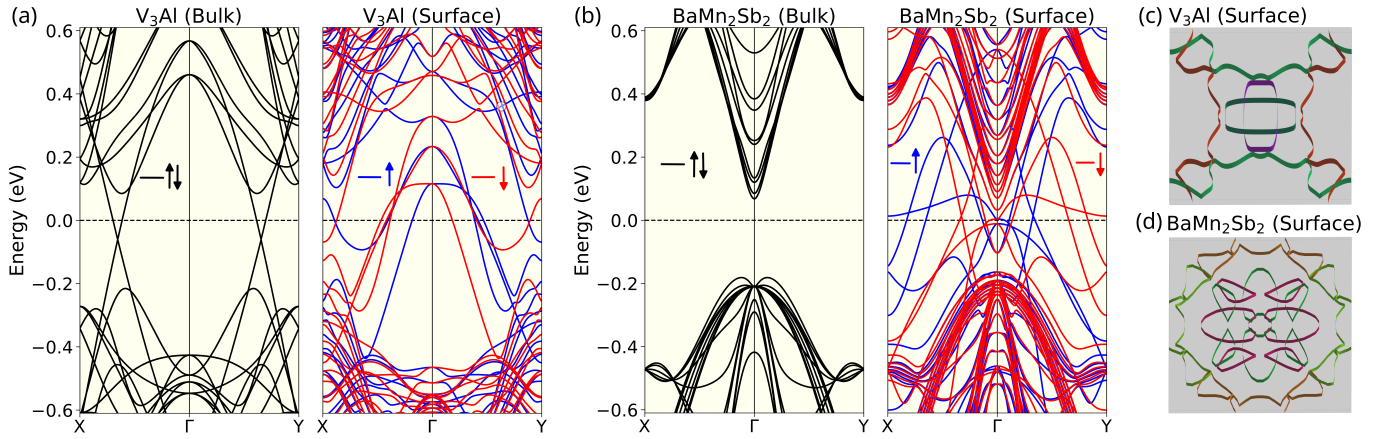


FIG. 2. Surface altermagnetic electronic structure of centrosymmetric AFMs. (a) Bulk and surface band structures of the G -type AFM V₃Al calculated along the in-plane X- Γ -Y high-symmetry path. The surface band structure is obtained from a 20-layer slab, while the bulk reference is calculated using a corresponding 20-layer bulk unit cell to enable direct comparison. The bulk bands are strictly spin-degenerate due to combined PT symmetry, whereas the surface bands exhibit pronounced nonrelativistic spin splitting in surface-localized states. (b) Same as (a), but for the G -type AFM BaMn₂Sb₂. (c), (d) Spin-resolved two-dimensional Fermi surfaces of the full slabs for V₃Al and BaMn₂Sb₂, respectively. The characteristic four-lobe angular dependence reflects the d -wave symmetry of the altermagnetic surface states.

derived bands cross the Fermi level, giving rise to a comparatively clean multi-lobed Fermi surface with alternating spin polarization. In contrast, several surface bands contribute near the Fermi level in V₃Al, resulting in a more complex Fermi-surface texture; for clarity, only two representative bands per spin channel are shown. Despite these material-specific differences, both systems exhibit a pronounced fourfold angular modulation with alternating spin character, providing a direct momentum-space signature of the d -wave symmetry imposed by the surface magnetic structure.

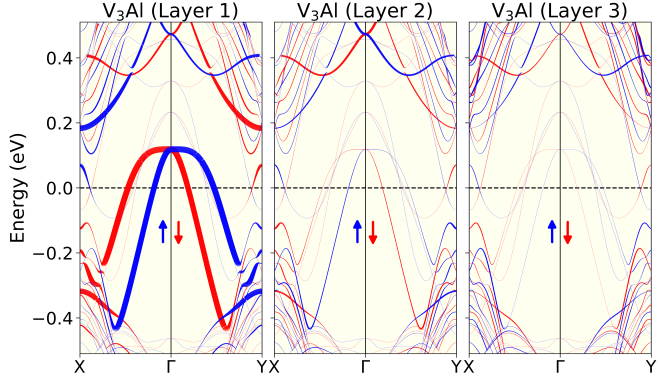


FIG. 3. Layer-resolved surface altermagnetic states in V₃Al. Fat-band representations of the asymmetric 20-layer V₃Al slab projected onto the first three magnetic V layers, shown along the in-plane X- Γ -Y path. The surface magnetic layer (Layer 1) hosts pronounced nonrelativistic d -wave altermagnetic spin splitting near the Fermi level with dominant spectral weight. The same split surface-derived states persist in the subsurface layers (Layers 2 and 3) with rapidly decreasing weight.

Having established the symmetry origin and momentum-space signatures of surface altermagnetism, we now turn to its spatial localization. Figure 3 presents layer-resolved fat-band representations for the asymmetric V₃Al slab, projected onto the first three magnetic V layers. The nonrelativistic d -wave spin splitting near the Fermi level is dominated by surface-derived states localized in the outermost magnetic layer, which carries the majority of the spectral weight. The same split surface bands persist in the subsurface layers with rapidly diminishing weight, while their dispersion and splitting remain unchanged. In deeper layers, surface-state contributions become negligible and the electronic structure recovers the spin degeneracy characteristic of the bulk. Because the surface states are metallic and partially delocalized, a unique layer-resolved energy splitting cannot be defined; instead, the progressive loss of spectral weight provides a direct and physically transparent measure of the decay of surface altermagnetism into the slab interior. An analogous behavior is found for BaMn₂Sb₂, as shown in the Supplemental Material [32].

This pronounced surface localization has several important consequences. First, it demonstrates that surface altermagnetism is not a reduced-dimensional bulk instability but a genuine surface phenomenon controlled by the local magnetic layer symmetry. Second, it explains the robustness of the effect with respect to slab thickness and interior structural details, provided that the surface termination induces magnetic sublattice inequivalence. Third, it implies that the same mechanism should operate at antiferromagnetic interfaces, where inversion symmetry is locally broken by contact with a dissimilar material. In particular, interfaces formed by cen-

etrosymmetric AFMs that host surface altermagnetism, such as V_3Al or $BaMn_2Sb_2$, with conventional semiconductors or insulators are expected to exhibit analogous exchange-driven d -wave altermagnetic states confined to the interfacial magnetic layers.

Finally, the symmetry-based criterion identified here provides a practical route for extending surface altermagnetism to a broad range of materials. Beyond the representative compounds discussed in the main text, many centrosymmetric collinear AFMs satisfy the necessary condition of magnetic sublattice inequivalence at specific surface terminations. An extended list of candidate materials spanning multiple structural families is provided in the Supplemental Material [32]. These findings establish surface altermagnetism as a general consequence of surface symmetry breaking in AFMs, substantially expanding the materials landscape of nonrelativistic altermagnetic systems. More broadly, the strong surface localization and purely exchange-driven nature of the effect suggest that surface altermagnetism should be readily accessible to experimental probes sensitive to surface electronic structure, such as angle-resolved photoemission spectroscopy and scanning tunneling microscopy. The same symmetry principle is expected to apply at antiferromagnetic interfaces and heterostructures, opening pathways toward engineering momentum-dependent spin polarization without net magnetization or SOC. Together, these results position surface altermagnetism as a versatile platform for exploring symmetry-controlled spin phenomena at antiferromagnetic surfaces and interfaces.

In summary, we establish surface altermagnetism as a symmetry-controlled phenomenon that can emerge at the surfaces of centrosymmetric collinear AFMs. By combining symmetry analysis with first-principles calculations, we show that surface inversion breaking alone, while necessary, is not sufficient to induce nonrelativistic spin splitting. Instead, surface altermagnetism arises only when the surface termination simultaneously breaks both combined PT and tT symmetries, thereby rendering the two antiferromagnetically coupled surface magnetic sublattices inequivalent. We demonstrate this mechanism explicitly for the G -type AFMs V_3Al and $BaMn_2Sb_2$, which host robust d -wave altermagnetic surface states despite fully spin-degenerate bulk electronic structures, and show that the same symmetry criterion is satisfied by a broad range of additional centrosymmetric AFMs spanning distinct structural families. In contrast, AFMs that preserve tT symmetry at the surface, remain spin-degenerate even when inversion symmetry is broken and the surface space groups are identical. The resulting altermagnetic surface states are strongly localized within the outermost magnetic layers, decay rapidly toward the interior, and arise entirely from exchange interactions without requiring SOC. Together, these results identify the simultaneous breaking of PT and tT at antiferromagnetic surfaces as the defining symmetry criterion for

realizing surface altermagnetism and provide a transparent framework for identifying and designing altermagnetic surfaces and interfaces, substantially expanding the materials platform for nonrelativistic spin-polarized electronic states in AFMs.

This work was supported by Deutsche Forschungsgemeinschaft (DFG): project 328545488 – CRC/ TRR 227, Project No. B12 and LO 1659/10-1.

DATA AVAILABILITY STATEMENT

Data available on request from the authors

* ersoy.sasioglu@physik.uni-halle.de

- [1] L. Šmejkal, R. González-Hernández, T. Jungwirth, and J. Sinova, Crystal time-reversal symmetry breaking and spontaneous hall effect in collinear antiferromagnets, *Science Advances* **6**, eaaz8809 (2020).
- [2] L. Šmejkal, J. Sinova, and T. Jungwirth, Beyond conventional ferromagnetism and antiferromagnetism: A phase with nonrelativistic spin and crystal rotation symmetry, *Physical Review X* **12**, 031042 (2022).
- [3] L. Šmejkal, A. H. MacDonald, J. Sinova, S. Nakatsuji, and T. Jungwirth, Anomalous hall antiferromagnets, *Nature Reviews Materials* **7**, 482 (2022).
- [4] Y. Guo, Y. Zhang, R. González-Hernández, L. Šmejkal, J. Sinova, and T. Jungwirth, Spin-split collinear antiferromagnets: A large-scale *ab initio* study, *Materials Today Physics* **32**, 100991 (2023).
- [5] I. I. Mazin, Altermagnetism in MnTe: Origin, predicted manifestations, and routes to detwinning, *Physical Review B* **107**, L100418 (2023).
- [6] T. Jungwirth, L. Šmejkal, J. Sinova, R. González-Hernández, *et al.*, Altermagnetic spintronics, arXiv preprint <https://doi.org/10.48550/arXiv.2508.09748> (2025), arXiv:2508.09748, 2508.09748.
- [7] N. Giuli, N. Bittner, M. T. Mercaldo, M. Cuoco, P. Gentile, S. M. Winter, and R. Valentí, Interaction-driven itinerant magnetism in altermagnets, *Phys. Rev. B* **111**, L020401 (2025).
- [8] Z. Feng *et al.*, An anomalous hall effect in altermagnetic ruthenium dioxide, *Nature Electronics* **5**, 735 (2022).
- [9] Z. Lin, D. Chen, W. Lu, X. Liang, S. Feng, K. Yamagami, J. Osiecki, M. Leandersson, B. Thiagarajan, J. Liu, *et al.*, Bulk band structure of RuO_2 measured with soft x-ray angle-resolved photoemission spectroscopy, *Phys. Rev. B* **111**, 134450 (2025).
- [10] S. Lee, S. Lee, S. Jung, J. Jung, D. Kim, Y. Lee, B. Seok, J. Kim, B. G. Park, L. Šmejkal, C.-J. Kang, and C. Kim, Broken kramers degeneracy in altermagnetic MnTe, *Phys. Rev. Lett.* **132**, 036702 (2024).
- [11] S. Reimers, L. Odenbreit, L. Šmejkal, V. N. Strocov, P. Constantinou, A. B. Hellenes, R. Jaeschke Ubiergo, W. H. Campos, V. K. Bharadwaj, A. Chakraborty, T. Denneulin, W. Shi, R. E. Dunin-Borkowski, S. Das, M. Kläui, J. Sinova, and M. Jourdan, Direct observation of altermagnetic band splitting in CrSb thin films, *Nat. Commun.* **15**, 2116 (2024).

[12] B. Jiang, M. Hu, J. Bai, Z. Song, C. Mu, G. Qu, W. Li, W. Zhu, H. Pi, Z. Wei, Y. Sun, Y. Huang, X. Zheng, Y. Peng, L. He, S. Li, J. Luo, Z. Li, G. Chen, H. Li, H. Weng, and T. Qian, A metallic room-temperature d-wave altermagnet, *Nat. Phys.* **21**, 754 (2025).

[13] N. Biniskos, M. dos Santos Dias, S. Agrestini, D. Sviták, K.-J. Zhou, J. Pospíšil, and P. Čermák, Systematic mapping of altermagnetic magnons by resonant inelastic x-ray circular dichroism, *Nature Communications* **16**, 9311 (2025).

[14] L.-D. Yuan, Z. Wang, J.-W. Luo, E. I. Rashba, and A. Zunger, Giant momentum-dependent spin splitting in centrosymmetric low-Z antiferromagnets, *Phys. Rev. B* **102**, 014422 (2020).

[15] J. Sødequist and T. Olsen, Two-dimensional altermagnets from high throughput computational screening: Symmetry requirements, chiral magnons, and spin-orbit effects, *Appl. Phys. Lett.* **124**, <https://doi.org/10.1063/5.0198285> (2024).

[16] B. Brekke, A. Brataas, and A. Sudbø, Two-dimensional altermagnets: Superconductivity in a minimal microscopic model, *Phys. Rev. B* **108**, 224421 (2023).

[17] R. Xu, Y. Gao, and J. Liu, Chemical design of monolayer altermagnets, *National Science Review* **13**, nwaf528 (2026).

[18] T. Jungwirth, J. Sinova, R. M. Fernandes, Q. Liu, H. Watanabe, S. Murakami, S. Nakatsuji, and L. Šmejkal, Symmetry, microscopy and spectroscopy signatures of altermagnetism, *Nature* **649**, 837 (2026).

[19] X. Wan, S. Mandal, Y. Guo, and K. Haule, High-throughput search for metallic altermagnets by embedded dynamical mean field theory, *Phys. Rev. Lett.* **135**, 106501 (2025).

[20] P.-H. Chang, I. I. Mazin, and K. D. Belashchenko, Inverse lieb materials: Altermagnetism and more, arXiv preprint arXiv:2508.04839 <https://doi.org/10.48550/arXiv.2508.04839> (2025).

[21] R. Bhattachari, P. Minch, and T. D. Rhone, High-throughput screening of altermagnetic materials, *Phys. Rev. Mater.* **9**, 064403 (2025).

[22] S. Brahimi, D. Prakash Rai, and S. Lounis, Confinement-induced altermagnetism in ruo₂ ultrathin films, *J. of Phys.: Condens. Matter* **37**, 395801 (2025).

[23] L. Bai, W. Feng, S. Liu, L. Šmejkal, Y. Mokrousov, and Y. Yao, Altermagnetism: Exploring new frontiers in magnetism and spintronics, *Advanced Functional Materials* **34**, 2409327 (2024).

[24] R. Tamang, S. Gurung, D. P. Rai, S. Brahimi, and S. Lounis, Altermagnetism and altermagnets: A brief review, *Magnetism* **5**, 17 (2025).

[25] J. Matsuda, H. Watanabe, and R. Arita, Multiferroic collinear antiferromagnets with hidden altermagnetic spin splitting, *Physical Review Letters* **134**, 226703 (2025).

[26] P. A. McClarty and J. G. Rau, Landau theory of altermagnetism, *Physical review letters* **132**, 176702 (2024).

[27] J. Sivianes, F. J. d. Santos, and J. Ibañez-Azpiroz, Optical signatures of spin symmetries in unconventional magnets, *Physical Review Letters* **134**, 196907 (2025).

[28] D. Jo, D. Go, Y. Mokrousov, P. M. Oppeneer, S.-W. Cheong, and H.-W. Lee, Weak ferromagnetism in altermagnets from alternating g-tensor anisotropy, *Physical review letters* **134**, 196703 (2025).

[29] R. M. Sattigeri, G. Cuono, and C. Autieri, Altermagnetic surface states: towards the observation and utilization of altermagnetism in thin films, interfaces and topological materials, *Nanoscale* **15**, 16998 (2023).

[30] E. I. Rashba, Properties of semiconductors with an extremum loop. i. cyclotron and combinational resonance in a magnetic field perpendicular to the plane of the loop, *Soviet Physics Solid State* **2**, 1109 (1960).

[31] G. Dresselhaus, Spin-orbit coupling effects in zinc blende structures, *Physical Review* **100**, 580 (1955).

[32] Supplemental material for "d-wave surface altermagnetism in centrosymmetric collinear antiferromagnets", <https://link.aps.org/supplemental/10.1103/PhysRevLett.XXX.YYYY>, contains computational details, additional figures, and extended materials classification.

[33] S. Smidstrup, T. Markussen, P. Vancraeyveld, J. Wellendorff, J. Schneider, T. Gunst, B. Verstichel, D. Stradi, P. A. Khomyakov, U. G. Vej-Hansen, M.-E. Lee, S. T. Chill, F. Rasmussen, G. Penazzi, F. Corsetti, A. Ojanperä, K. Jensen, M. L. N. Palsgaard, U. Martinez, A. Blom, M. Brandbyge, and K. Stokbro, QuantumATK: an integrated platform of electronic and atomic-scale modelling tools, *J. Phys.: Condens. Matter* **32**, 015901 (2019).

[34] J. P. Perdew, K. Burke, and M. Ernzerhof, Generalized gradient approximation made simple, *Phys. Rev. Lett.* **77**, 3865 (1996).

[35] M. J. Van Setten, M. Giantomassi, E. Bousquet, M. J. Verstraete, D. R. Hamann, X. Gonze, and G.-M. Rignanese, The PseudoDojo: Training and grading a 85 element optimized norm-conserving pseudopotential table, *Comput. Phys. Commun.* **226**, 39 (2018).

[36] I. Galanakis, S. Tirpanci, K. Özdogan, and E. Şaşioğlu, Itinerant g-type antiferromagnetism in d 0 3-type v 3 z (z= al, ga, in) compounds: A first-principles study, *Physical Review B* **94**, 064401 (2016).

[37] S. Khmelevskyi, First-principles modeling of longitudinal spin fluctuations in itinerant electron antiferromagnets: High néel temperature in the V₃Al alloy, *Phys. Rev. B* **94**, 024420 (2016).

[38] M. Tas, E. Şaşioğlu, C. Friedrich, S. Blügel, and I. Galanakis, Design of L₂1-type antiferromagnetic semiconducting full-heusler compounds: A first principles DFT+GW study, *J. Appl. Phys.* **121**, <https://doi.org/10.1063/1.4975351> (2017).

[39] X. Chen, Y. Huang, J. Liu, H. Yuan, and H. Chen, Effects of Ga substitution on electronic and thermoelectric properties of gapless semiconductor V₃Al, *RSC advances* **9**, 3847 (2019).

[40] J. An, A. S. Sefat, D. J. Singh, and M.-H. Du, Electronic structure and magnetism in BaMn₂As₂ and BaMn₂Sb₂, *Phys. Rev. B* **79**, 075120 (2009).

[41] N. S. Sangeetha, V. Smetana, A.-V. Mudring, and D. C. Johnston, Antiferromagnetism in semiconducting SrMn₂Sb₂ and BaMn₂Sb₂ single crystals, *Phys. Rev. B* **97**, 014402 (2017).

[42] Q. Zhang, Z. Diao, H. Cao, A. Saleheen, R. Rishi, A. Sapkota, *et al.*, Structure-property relationship in layered BaMn₂Sb₂ and Ba₂Mn₃Sb₂O₂, *Physical Review B* **99**, 184416 (2019).